

# Lithospheric scale gravitational flow: the impact of body forces on orogenic processes from Archaean to Phanerozoic

PATRICE F. REY<sup>1</sup> & GREGORY HOUSEMAN<sup>2</sup>

<sup>1</sup>*School of Geosciences, The University of Sydney, NSW 2006 and Dept. de Géologie, UMR-CNRS 6524, Université Jean Monnet, St Etienne, F42023, France*

<sup>2</sup>*School of Earth and Environment, University of Leeds, Leeds, LS2 9JT, UK*

**Abstract:** In the Archaean, the combination of warmer continental geotherm with a lighter sub-continental lithospheric mantle suggests that gravitational forces played a more significant role in continental lithospheric deformation. To test this hypothesis, we compare the evolution of the deformation and the regional state of stress in 'Archaean-like' and 'Phanerozoic-like' lithospheres submitted to the same boundary conditions in a triaxial stress-field with imposed convergence in one direction. For plausible physical parameters, thickening of normal to cold Phanerozoic lithospheres produces relatively weak buoyancy forces, either extensional or compressional. In contrast, for Archaean continental lithospheres, or for anomalously warm Phanerozoic lithospheres, lateral gravitationally-driven flow prevents significant thickening. This conclusion is broadly consistent with: (1) the relative homogeneity of the erosional level now exposed at the surface of Archaean cratons, (2) the sub-aerial conditions that prevailed during the emplacement of up to 20 km of greenstone cover, (3) the relatively rare occurrence in the Archaean record of voluminous detrital sediments, (4) the near absence of significant tectonic, metamorphic and magmatic age gradients across Archaean cratons, (5) the relative homogeneity of strain across large areas, and (6) the ubiquitous presence of crustal-scale strike slip faults in many Late Archaean cratons.

One of the most contentious issues in Archaean geology is the significance of the particular features seen in the surface geology of most Archaean cratons. These involve the characteristic strain pattern of domes and basins; the ubiquity (in particular in Late-Archaean cratons) of strike-slip faults; the relative homogeneity at the craton scale of the finite strain field, the metamorphic facies and the erosion level; together with the particular timing of tectonics, magmatism, and metamorphism that seem to develop craton-wide within a very narrow time window (Binns *et al.* 1976; Choukroune *et al.* 1997; Galer & Mezger 1998; Hamilton 1998; Qiu *et al.* 1999; Rey *et al.* 2003). Based on the same field evidence, these features are interpreted by some authors as evidence of plate-tectonic processes (e.g., Snowden & Bickle 1976; Myers & Watkins 1985; Treloar & Blenkinsop 1995), and by others as evidence of gravitational instabilities (McGregor 1951; Collins 1989; Ramsay 1989; Jelsma *et al.* 1993; Bouhallier *et al.* 1993; Chardon *et al.* 1998) possibly related to plume activity (Choukroune *et al.* 1995; Warren & Ellis 1996). In this three-decade-long ongoing debate, the differences in mechanical behaviour of Phanerozoic and

Archaean continental lithospheres have not been properly considered, yet regional finite strain fields depend significantly on the thermo-mechanical properties of the continental lithosphere. Consequently, the particular features observed in Archaean cratons could be related, in part, to contrasting lithospheric mechanical properties rather than to contrasting tectonic processes.

In this paper we aim to illustrate the relatively greater importance of gravitational forces in the tectonic evolution of ancient continental lithospheres. Based on triaxial numerical experiments that compare the evolution of Phanerozoic-like and Archaean-like lithospheres under horizontal convergence, we show that ancient continental lithospheres could have been under an increased stabilizing influence of gravitational forces that promoted homogeneous deformation and therefore impeded the development of strain localization along linear belts. If the buoyancy-derived stress were greater in the Archaean, then lateral escape (strike-slip faults and crustal-scale lateral crustal flow) rather than large-scale thrust and thickening could have become the primary response to tectonic convergence. We also suggest that the secular cooling

of the continental geotherm, combined with the decrease in the buoyancy of the sub-continental lithospheric mantle (SCLM), have changed the thermo-mechanical properties of the continental lithosphere in such a way that the impact of gravitational forces on lithospheric deformation has decreased over geological time.

### Argand Ratio: assessing the impact of gravitational forces on modern and ancient continental lithospheres

Scaled models of orogenic systems depend on a few dimensionless parameters that describe the relative importance of different processes in the stress and thermal balance. Amongst these parameters the Argand Ratio characterizes the ability of gravitational forces to intervene in lithospheric deformation (Fig. 1). The Argand Ratio ( $AR$ ) can be defined as the local ratio of the gravitational stress (arising from lateral variation of gravitational potential energy and thus of density) to the averaged lithospheric strength at a nominal strain rate (i.e., the stress-driving deformation). The ratio  $AR$  may be compared with the Argand Number ( $Ar$ ) of England & McKenzie (1982, 1983), a global parameter by which one can quantify the overall regional balance between gravitational stress and viscous stress in an indentation problem (see also Houseman & England 1986; Buck & Soukoutis 1994; Schmalholz *et al.* 2002, 2005).  $AR$  is obtained from  $Ar$  by replacing the nominal buoyant stress factor in  $Ar$  with the locally variable buoyant stress (relative to a reference column), and similarly replacing the nominal viscous stress scale factor in  $Ar$  with the locally variable strength of the lithosphere. The resulting Argand Ratio can be used to describe the evolution during deformation of the balance between buoyant stress and the strength of the lithosphere. The Argand Ratio measures the tendency of the lithosphere to deform in response to the variation of gravitational potential energy ( $\Delta GPE$ ), and therefore is a measure of the ability of gravitational forces to intervene in lithospheric deformation.

In modern continental lithospheres, the Argand Ratio may reach values  $\geq 1$  when large  $\Delta GPE$  exists and/or when the orogenic system involves a weak lithosphere (i.e., a warmer geotherm). In Tibet as well as in the Basin and Range Province of the western USA, it has been argued that present-day crustal flow is strongly influenced by forces induced by large gradients in gravitational potential energy (England & Molnar 1997; Jones *et al.* 1996;

Flesch *et al.* 2000). A warmer geotherm reduces the strength of the continental lithosphere and, as a rule of thumb, it is inferred that a thickened continental crust spreads under its own weight (i.e., Argand Ratio  $\geq 1$  for a given effective strain rate) when the temperature at the Moho is above *c.* 700°C (e.g., Sonder *et al.* 1987).

In modern continental lithospheres, such a thermal condition is likely to be transient and associated with either crustal thickening or the rise of the lithosphere/asthenosphere interface under continental areas. In the Archaean however, the larger radiogenic heat production, possibly coupled with a stronger basal heat flow, would lead to warmer continental geotherms. For radiogenic-element contents compatible with the present-day average composition of Archaean cratons (Taylor & McLennan 1986) and plausible mantle heat flow, the steady state temperature at the Moho in the Late Archaean could have been close to 700°C (Rey *et al.* 2003). In fact, one can argue that this temperature could have buffered the thickness of the continental crust, since a thicker crust would have spread (Bailey 1999). Hence, the Archaean continental lithosphere would have been less likely to develop large gradients of crustal thickness. In addition, there is solid evidence that the buoyancy of Archaean continental lithosphere was enhanced by a sub-continental lithospheric mantle, more depleted, and therefore less dense, than that of Phanerozoic lithosphere (3310 kg m<sup>-3</sup> vs 3370 kg m<sup>-3</sup>, Griffin *et al.* 1998). Upon lithospheric thickening, a more buoyant sub-continental lithospheric mantle would produce relatively greater extensional forces, and therefore a larger Argand Ratio. Figure 1a illustrates the consequences of a warmer geotherm on the integrated strength of the lithosphere (i.e., the denominator of  $AR$ ). Figure 1b illustrates the effect of a more buoyant lithospheric mantle on the local gravitational stress (i.e., the numerator of  $AR$ ). Both effects imply that local gravitational forces might have been more important relative to in-plane stresses arising from distant plate boundaries in the Archaean than in the Phanerozoic.

### Models: assumptions and simplifications

Keeping in mind that our objective is to illustrate the difference in lithospheric deformation due to contrasting buoyancy and thermal structure, we assume here that Archaean-like and Phanerozoic-like lithospheres are similar in all but two aspects: the density profile and the temperature profile. There are a number of problems when

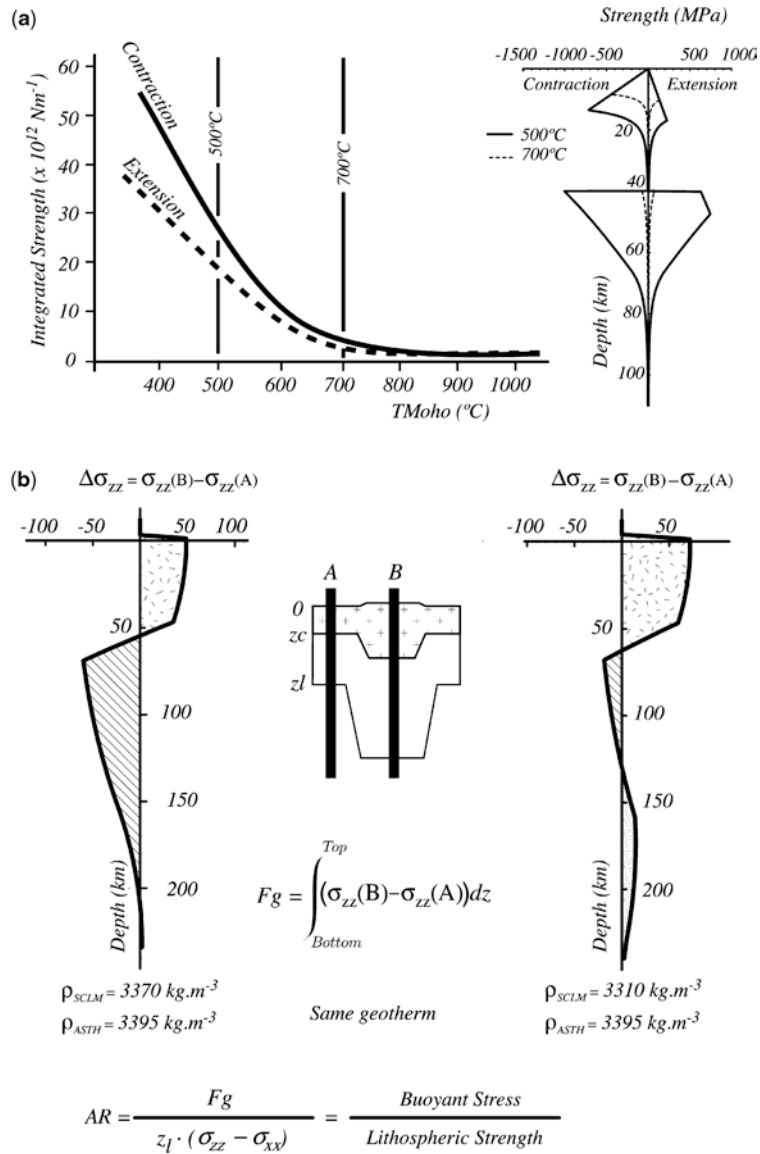


**Fig. 1.** (a) Consequences of a warmer geotherm on the strength of continental lithosphere and therefore on the  $AR$  denominator, and (b) consequences of a more buoyant sub-continental lithospheric mantle on the gravitational force related to homogeneous thickening and therefore on the  $AR$  numerator. (a) The temperature at the Moho is used as a proxy for the continental geotherm. As the temperature at the Moho increases, the integrated strength of the continental lithosphere (integration with depth of the rheological profile) decreases linearly until the Moho reaches c.  $700^{\circ}\text{C}$ . Above this temperature, the integrated strength does not change much as the strength of the upper crust, which is now the stronger layer of the lithosphere, is less sensitive to temperature. In inset, the rheological profiles for  $T_{\text{Moho}} = 500^{\circ}\text{C}$  and  $700^{\circ}\text{C}$  showing the disappearance of the strong upper mantle in warm continental lithospheres. (b) Upon doubling the thickness of a lithospheric column via homogeneous thickening, a gravitational force is created. The gravitational force ( $Fg$ ) is given by the integration with depth of the difference in the lithostatic pressure ( $\Delta\sigma_{zz}$ ) between the deformed (column B) and the reference lithosphere (column A). Upon thickening, a heavy SCLM generates a deficit in gravitational potential energy (hatched areas in left profile) that balances the excess in gravitational potential energy (stippled areas) in the upper lithosphere. In contrast, a less dense SCLM reduces the gravitational force stored in the lower lithosphere (right profile) but increases the gravitational potential energy stored in the upper lithosphere. Hence, the overall gravitational force created by homogeneous thickening of a lithosphere with a buoyant lithospheric mantle is much larger than that created by the homogeneous thickening of a lithosphere with a denser lithospheric mantle.

trying to define average continental lithospheres representative of Archaean and Phanerozoic eons. Firstly, there is a much larger reduction in crustal radiogenic heat production within the Archaean Eon alone than from the end of the Archaean to now. Secondly, Phanerozoic lithospheres exist in a very large range of thermal regimes. We must account for variation in the properties of both Archaean and Phanerozoic continental lithospheres, for probable systematic differences between the average properties, and for significant overlap in the ranges of properties of the two types of lithosphere. Therefore, we define three Archaean and three Phanerozoic model lithospheres covering a plausible range of thermal regimes (Table 1). Table 2 summarizes the relevant thermo-mechanical parameters.

### Density structure

In all models, the continental crust has the same thickness,  $z_c$  (40 km) and the same depth-dependent density structure, defined at 0°C. For the crust, the density is assumed to increase from the top of the crust ( $\rho_a$ ) to the Moho ( $\rho_b$ ) because of a compositional gradient. In addition, it is dependent on temperature ( $\alpha_c$  is the coefficient of thermal expansion).

$$\rho_{\text{crust}}(z) = \left[ \rho_a + \left( \frac{\rho_b - \rho_a}{z_c} \right) \cdot z \right] \times (1 - \alpha_c \cdot T(z)) \quad (1)$$

Because of a larger degree of depletion, the density of the sub-continental lithospheric mantle (SCLM) was most likely lower in the Archaean (Jordan 1975, 1997; Griffin *et al.* 1998). Following Griffin *et al.* (1998), the density at 0°C of the SCLM in the Archaean and Phanerozoic models are  $3310 \text{ kg m}^{-3}$  and  $3370 \text{ kg m}^{-3}$  respectively. We assume that the asthenospheric mantle acts as an infinite reservoir with constant density through time

$\rho_{ao} = 3395 \text{ kg m}^{-3}$ ). Assumed pressure- and temperature-dependences for the lithospheric mantle density are defined by:

$$\rho_{lm}(z) = \rho_{lmo} \cdot (1 - \alpha_m \cdot T(z) + \chi_m \cdot P) \quad (2)$$

where  $\chi_m$  is the coefficient of compressibility,  $P$  is the pressure, and  $\rho_{lmo}$  is the density of lithospheric mantle at 0°C. For the density profile in the asthenosphere, the density of the asthenosphere  $\rho_{ao}$  at 0°C is substituted for  $\rho_{lmo}$  in equation (2), with constant temperature equal to that at the base of the lithosphere, and the same value of  $\chi_m$ .

### Continental geotherm

The temperature profile is calculated from a two-layer model with no radiogenic heat production in the SCLM and a depth-independent radiogenic heat production in the crust of thickness  $z_c$ . The steady state and transient geotherms are derived from the one-dimensional diffusion-advection equation:

$$\frac{\partial T}{\partial t} = \kappa \cdot \frac{\partial^2 T}{\partial z^2} + \frac{H}{\rho \cdot cp} - v \cdot \frac{\partial T}{\partial z} \quad (3)$$

where  $\kappa$  thermal diffusivity;  $H$  is the radiogenic heat production;  $\rho$  is the density;  $cp$  is the heat capacity; and  $v$  is the velocity of the medium relative to the upper surface. For boundary conditions we assume a constant mantle heat flow entering the base of the lithosphere, and a constant temperature (25°C) at the top of the crust. During deformation, the mantle heat flow remains constant and is applied to the base of the lithosphere, which is defined by the isotherm 1330°C.

For Archaean-like lithospheres, we conservatively choose a crustal radiogenic heat production representative of the Late Archaean. Using the average concentration in radiogenic elements for present-day Archaean cratons

**Table 1.** Vertical geometry and thermal parameters for our models of Phanerozoic-like and Archaean-like continental lithospheres

	$z_c$ (km)	$H$ ( $10^{-6} \text{ Wm}^{-3}$ )	$Q_o$ ( $10^{-3} \text{ Wm}^{-2}$ )	$z_l$ (km)	$T_{\text{Moho}}$ (°C)
Phan160	40	0.48	18.7	160	447
Phan120	40	0.48	24.95	120	546
Phan80	40	0.48	37.4	80	741
Arch160	40	0.99	16.2	160	566
Arch120	40	0.99	21.6	120	652
Arch80	40	0.99	32.3	80	820

Abbreviations:  $z_c$ : crustal thickness;  $H$ : Crustal radiogenic heat production (depth independent);  $Q_o$ : Basal heat flow;  $z_l$ : Depth of the isotherm 1330°C, base of the lithosphere;  $T_{\text{Moho}}$ : Temperature at the Moho.

**Table 2.** List of parameter values

Parameters	Values	Units
Gravity: $g$	9.81	$\text{m s}^{-2}$
Crust thermal expansion: $\alpha_c$	$3.5 \times 10^{-5}$	$\text{K}^{-1}$
Mantle thermal expansion: $\alpha_m = a_0 + a_1T + a_2T^{-2}$	$a_0 = 2.697 \times 10^{-5}$ $a_1 = 1.0192 \times 10^{-8}$ $a_2 = -0.1282$	$\text{K}^{-1}$
Mantle bulk modulus: $\chi_m$	130	GPa
Lithosphere thermal diffusivity: $\kappa$	$0.97 \times 10^{-6}$	$\text{m}^2 \text{s}^{-1}$
Crust volumetric heat production: $H_c$	cf. Table 1	$\text{Wm}^{-3}$
Mantle volumetric heat production: $H_m$	0	$\text{Wm}^{-3}$
Heat capacity: $cp$	1000	$\text{J kg}^{-1} \text{K}^{-1}$
Surface temperature: $T_o$	293	K
Temperature at the base of the lithosphere: $T_l$	1603	K
Heat flow at the base of the lithosphere: $Q_o$	cf. Table 1	$\text{Wm}^{-2}$
Crustal thickness: $z_c$	cf. Table 1	km
Lithosphere thickness: $z_l$	cf. Table 1	km
Lithospheric mantle density @ $T = 0^\circ\text{C}$ : $\rho_{lmo}$	Arch: 3310, Phan: 3370	$\text{kg m}^{-3}$
Asthenospheric mantle density @ $T = 0^\circ\text{C}$ : $\rho_{ao}$	3395	$\text{kg m}^{-3}$
Upper crust mass density @ @ $T = 0^\circ\text{C}$ : $\rho_a$	2700	$\text{kg m}^{-3}$
Lower crust mass density @ @ $T = 0^\circ\text{C}$ : $\rho_b$	2900	$\text{kg m}^{-3}$
Water mass density: $\rho_w$	1030	$\text{kg m}^{-3}$
Ratio pore pressure to overburden stress: $\lambda$	0.36	
Universal gas constant: $R$	8.3144	$\text{J mol}^{-1} \text{K}^{-1}$
Crust power law sensitivity: $n_c$	3	
Crust power law activation enthalpy: $Q_c$	190000	$\text{J mol}^{-1}$
Crust power law pre-exponent: $A$	$5 \times 10^{-6}$	$\text{MPa}^{-n} \text{s}^{-1}$
Mantle power law sensitivity: $n_m$	3	
Mantle power law activation enthalpy: $Q_m$	520000	$\text{J mol}^{-1}$
Mantle power law pre-exponent: $A_m$	$7 \times 10^4$	$\text{MPa}^{-n} \text{s}^{-1}$
Mantle Dorn plasticity activation enthalpy: $Q_d$	540000	$\text{J mol}^{-1}$
Mantle Dorn plasticity law stress threshold: $\sigma_d$	8500	MPa
Mantle Dorn plasticity law strain rate: $\varepsilon_d$	$3.05 \times 10^{11}$	$\text{s}^{-1}$

(Taylor & McLennan 1986) one can work out the crustal radiogenic heat production 2.7 Ga ( $0.99 \times 10^{-6} \text{ Wm}^{-3}$ ). For Phanerozoic-like lithospheres, we chose the present-day average crustal radiogenic heat content of Archaean crusts ( $0.48 \times 10^{-6} \text{ Wm}^{-3}$ ). We assume for simplicity that the bases of the thermal, mechanical and compositional lithospheres are all coincident. The mantle heat flow controls,  $z_l$  the thickness of the lithosphere (i.e., the depth of the isotherm  $1330^\circ\text{C}$ ). This is highly variable in Phanerozoic lithospheres, and was most likely highly variable in the Archaean too (Lenardic & Moresi 2000). We chose mantle heat flows to get three Archaean-like models (Arch80, Arch120 and Arch160) and three Phanerozoic-like models (Phan80, Phan120 and Phan160) with nominal equilibrium lithospheric thicknesses of 80, 120, and 160 km respectively (Fig. 2, Table 1). Consequently, the Moho temperature for Phanerozoic-like lithosphere with assumed crustal thickness of 40 km ranges from  $447^\circ\text{C}$  (Phan160), to  $546^\circ\text{C}$  (Phan120), to  $741^\circ\text{C}$

(Phan80). Phan80 represents an anomalously warm and thin continental lithosphere, while Phan160 represents a cold and thick lithosphere. The Moho temperature of the Archaean-like models varies from  $566^\circ\text{C}$  (Arch160), to  $652^\circ\text{C}$  (Arch120), to  $820^\circ\text{C}$  (Arch80). Arch80 is clearly an anomalously hot and thin continental lithosphere with a Moho temperature in excess of what would be required for lower crustal flow.

#### Constitutive equations and rheological profile

We consider here the thin viscous sheet equations in a triaxial situation in which we specify that the horizontal principal stresses,  $\sigma_{xx}$  and  $\sigma_{yy}$ , are externally specified while the vertical stress component,  $\sigma_{zz}$ , is determined simply by gravity. All quantities represent vertical averages through the lithospheric column. Expressed in terms of differential stresses, and

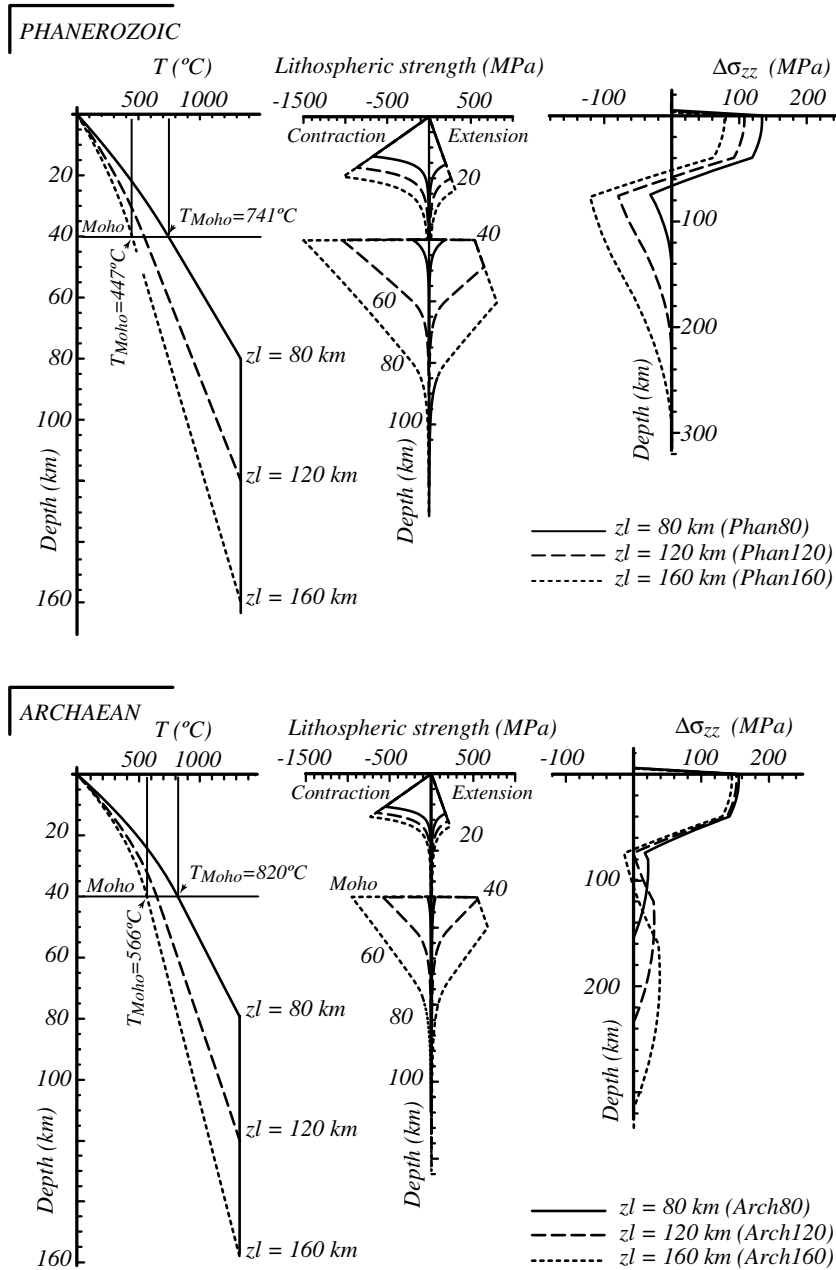


**Fig. 2.** Definition of Phanerozoic-like and Archaean-like lithosphere models. Moho temperatures of Archaean models are systematically greater by  $c. 100^{\circ}\text{C}$  than Phanerozoic models ( $566\text{--}820^{\circ}\text{C}$  vs  $447\text{--}741^{\circ}\text{C}$ ). Hence, the Archaean models have a reduced strength when compared to the Phanerozoic models. Rheological profiles show that Phan160 and Arch120 have a strong upper mantle whereas Phan80 and Arch80 have a weak upper mantle. The contrasting density structure impacts on the gravitational force, as shown by plotting the  $\Delta\sigma_{zz}$  profile for each model, assuming homogeneous doubling of the lithosphere thicknesses. In Archaean models, excesses in gravitational potential energy are stored in both crustal and mantle layers. For Phan80, the  $\Delta\sigma_{zz}$  profile is similar to Archaean profiles in the sense that there is a large, unbalanced excess in gravitational potential energy (GPE) in the upper part of the lithosphere. In contrast, for the  $\Delta\sigma_{zz}$  profile of Phan160, the deficit in gravitational energy in the lower lithosphere is greater than the excess in GPE in the upper lithosphere.

assuming isotropy for simplicity, the constitutive equations can be expressed as:

$$\sigma_{xx} - \sigma_{yy} = 2\eta \cdot (\dot{\epsilon}_{xx} - \dot{\epsilon}_{yy}) \quad (4)$$

$$\sigma_{zz} - \sigma_{yy} = 2\eta \cdot (\dot{\epsilon}_{zz} - \dot{\epsilon}_{yy}) \quad (5)$$

$$\sigma_{zz} - \sigma_{xx} = 2\eta \cdot (\dot{\epsilon}_{zz} - \dot{\epsilon}_{xx}) \quad (6)$$

where  $\eta$  represents the depth-averaged effective isotropic viscosity, which includes the frictional Byerlee's law relation in the brittle layer and ductile stress laws in the lower layer as summarized below. Noting that the medium is effectively incompressible:  $\dot{\epsilon}_{xx} + \dot{\epsilon}_{yy} + \dot{\epsilon}_{zz} = 0$ , then the three unknown strain-rates under the prescribed triaxial stress field are given by:

$$\dot{\epsilon}_{zz} = \frac{1}{6\eta} \cdot (2\sigma_{zz} - \sigma_{xx} - \sigma_{yy}) \quad (7)$$

$$\dot{\epsilon}_{yy} = \frac{1}{6\eta} \cdot (2\sigma_{yy} - \sigma_{zz} - \sigma_{xx}) \quad (8)$$

$$\dot{\epsilon}_{xx} = \frac{1}{6\eta} \cdot (2\sigma_{xx} - \sigma_{zz} - \sigma_{yy}) \quad (9)$$

The effective viscosity is obtained by calculating the resistance to deformation at a specified strain-rate (assumed constant with depth) by evaluating the vertically integrated strength of the lithosphere:

$$\text{Integrated Strength} = \int_{\text{bottom}}^{\text{top}} (\sigma_1(z) - \sigma_3(z)) \cdot dz \quad (10)$$

We use the standard rheological profile of Brace & Kohlstedt (1980) for the continental lithosphere, in which frictional sliding is the dominant failure mechanism at low temperature and high strain rate (in the upper crust and the upper mantle, Sibson 1974):

$$\sigma_1(z) - \sigma_3(z) = \beta \cdot \rho(z) \cdot g \cdot z \cdot (1 - \lambda) \quad (11)$$

where  $g$  is the gravitational acceleration;  $\lambda$  is the ratio of fluid pore pressure to the normal stress; and  $\beta$  is a parameter dependent on the type of faulting, therefore dependent on the tectonic regime. It is given by:

$$\beta = \frac{R - 1}{1 + \delta \cdot (R - 1)} \quad (12)$$

with

$$R = \left( \sqrt{1 + \mu^2} + \mu \right)^{-2}$$

and

$$\delta = \frac{\sigma_{zz} - \sigma_3}{\sigma_1 - \sigma_3} \quad (13)$$

and  $\mu$  the coefficient of internal friction (*cf.* Houseman & England 1986; Ranalli 1995). As the differential stress ratio  $\delta$  varies from 0 (when  $\sigma_{zz} = \sigma_3$ ) to 1 (when  $\sigma_{zz} = \sigma_1$ ),  $\beta$  varies from 3 (reverse faults) to 0.75 (normal faults) for  $\mu = 0.75$ . Intermediate  $\beta$  values describe oblique slip faulting with  $3 < \beta < 1.2$  for transpression, and  $1.2 < \beta < 0.75$  for transtension. Strike-slip faulting occurs for  $\beta = 1.2$  (when  $\sigma_{zz} = (\sigma_1 + \sigma_3)/2$ ). Although different mechanisms (e.g., thrusting and strike-slip faulting) may occur simultaneously in a general triaxial stress-field, our calculation of the effective isotropic viscosity must assume a single value of  $\beta$ , which is determined from the current differential stress ratio  $\delta$ .

At high temperatures and differential stresses below 200 MPa, the viscous deformation of the crust and the mantle is modelled as power law creep (Evans & Goetze 1979). The creep is thermally activated (Ranalli 1995) and may be written in terms of the second invariant of the strain-rate tensor  $\dot{E}^2 = (\sum_{i,j} \dot{\epsilon}_{ij} \cdot \dot{\epsilon}_{ij}/2)$  as follows:

$$(\sigma_{ii} - \sigma_{jj}) = \left[ \left( \frac{2}{3} \right)^{(n+1)/2n} A^{-1/n} \dot{E}^{(1-n)/n} \times \exp\left( \frac{Q}{n \cdot R \cdot T} \right) \right] (\dot{\epsilon}_{ii} - \dot{\epsilon}_{jj}) \quad (14)$$

The numerical factor in (14) is introduced so that  $A$  values determined for uniaxial compression experiments can be used in a general triaxial formulation which is independent of the orientation of the axes (Molnar *et al.* 1998).

Finally, at differential stresses larger than 200 MPa we use a Dorn flow law (Evans & Goetze 1979):

$$\sigma_{ii} - \sigma_{jj} = \sigma_d \left[ 1 - \sqrt{\frac{R \cdot T(z)}{Q_d} \cdot \ln\left( \frac{\dot{\epsilon}_d}{\dot{\epsilon}_{ii}} \right)} \right] \quad (15)$$

where  $\sigma_d$ , the so-called Peierls stress, is the yield stress needed to move crystal dislocations at  $T = 0$  K. This experimental law limits the strength of the upper mantle to realistic values at high strain rates. We thus define an effective viscosity for the whole system by first integrating the stress difference as a function of depth through the lithosphere (using the different

deformation mechanisms that apply in the relevant depth ranges) and dividing by twice the strain-rate difference (compare Eqns 4–6).

### Boundary conditions

The model lithospheres are set up in dynamic equilibrium, assuming that the two horizontal principal stress components are initially equal to the vertical principal stress component as determined from the initial density column (each component depth-averaged). The tectonic effect of in-plane stress in the  $x$ -direction from a remote plate boundary is then simulated by adding to the stress component,  $\sigma_{xx}$ , an increment that is great enough to drive convergence at an initial strain rate of  $5 \times 10^{-15} \text{ s}^{-1}$ . Under this tectonic driving force, thin sheet deformation (England & McKenzie 1982, 1983) occurs, and the tectonic stress balance changes with the thickness of the deforming lithosphere. Disregarding erosion and sedimentation, the lithospheric column changes under the action of (1) a triaxial state of stress, (2) local isostasy, and (3) thermal relaxation. These processes are integrated forward in time, using small increments of time whose duration is such that the incremental change in crustal thickness is kept below 250 m and that of the entire lithosphere to under 500 m. Calculation of transient geotherms uses a Crank-Nicholson finite differences scheme with a constant heat flow at the base of the lithosphere and no lateral heat transfer. Deformation strain rates are calculated using the thin sheet approximation, in which the vertically averaged stress-difference is related to the strain rates by the constitutive equations incorporated into Equation (10). The vertical stress-component is always evaluated directly from the current density profile. The two horizontal stress-components are set up as described above:  $\sigma_{yy}$  is constant throughout the experiments and equal to its initial value;  $\sigma_{xx}$  results from maintaining a constant plate boundary force against the vertical section of the deforming lithosphere normal to the  $x$ -direction. Therefore,  $\sigma_{xx}$  is inversely proportional to the current thickness of the deforming lithosphere on which the force is applied.

### Presentation of the results

The evolution of our six model lithospheres, subject to the above boundary conditions, is presented in Figures 3 to 5. Figure 3 gives the position through time of the three main density interfaces: the surface, the Moho, and the base of the lithosphere (i.e., the isotherm  $1330^\circ\text{C}$ ).

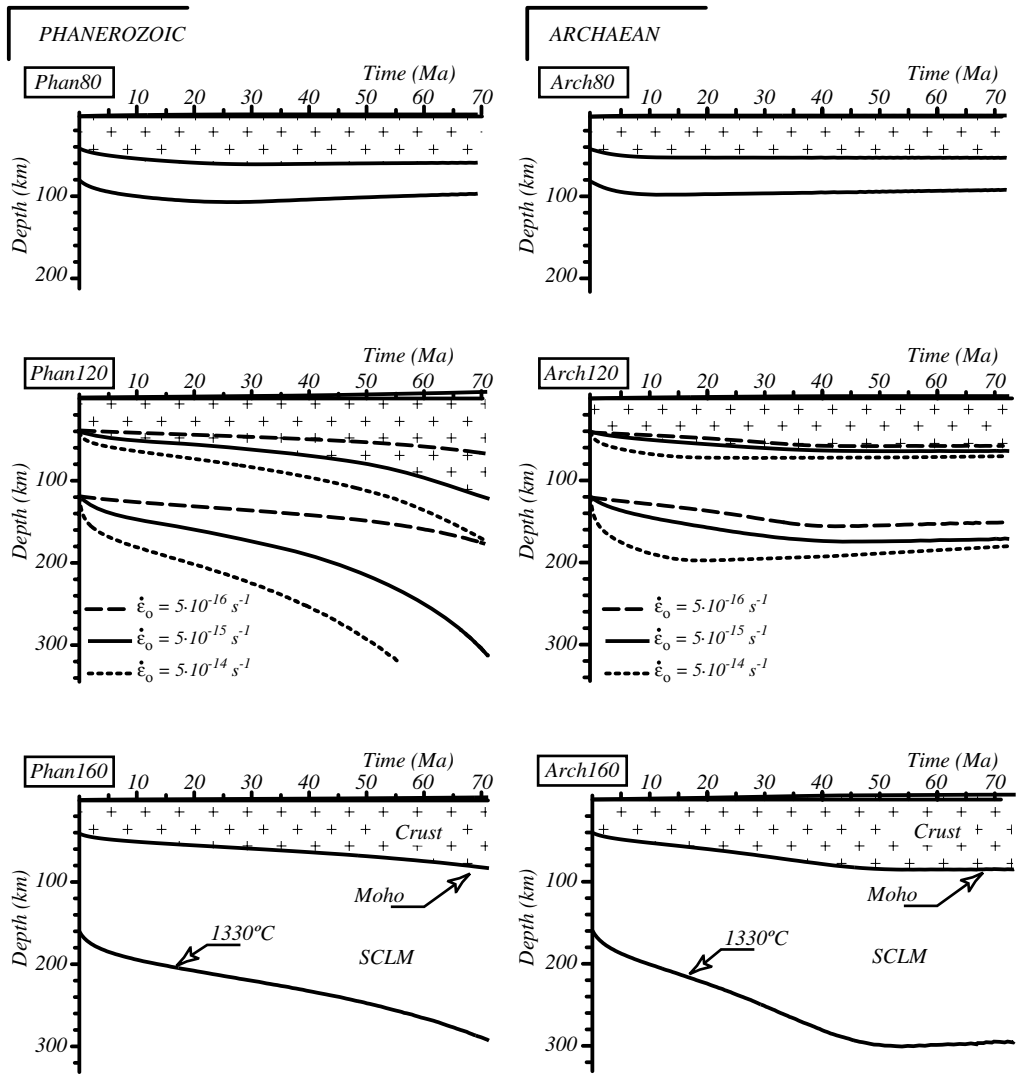
Hence, it illustrates the evolution of the crustal and lithospheric thicknesses during convergence. Figure 4 shows the evolution of the magnitude of the differential stresses ( $\sigma_{zz} - \sigma_{xx}$ ) versus ( $\sigma_{zz} - \sigma_{yy}$ ). In this graph, four domains can be identified, a domain in which extension occurs in both horizontal directions ( $(\sigma_{zz} - \sigma_{xx}) > 0$  and  $(\sigma_{zz} - \sigma_{yy}) > 0$ , therefore  $\sigma_{zz} = \sigma_1$ ); a domain in which convergence occurs in both horizontal directions ( $(\sigma_{zz} - \sigma_{xx}) < 0$  and  $(\sigma_{zz} - \sigma_{yy}) < 0$ , hence  $\sigma_{zz} = \sigma_3$ ); and the two transcurent domains in which there is a combination of extension in one direction and convergence in the other ( $\sigma_{zz} = \sigma_2$ ).

Figure 4 can also be contoured for the Argand Ratio. We have defined the Argand Ratio as the ratio of the gravitational stress to the depth-averaged strength of the lithosphere at a nominal strain rate. Assuming local isostatic compensation, and disregarding flexural stresses and shear tractions at the base of the lithosphere, the gravitational stress is the depth average of ( $\sigma_{zz} - \sigma_{yy}$ ). It is the difference between the averaged lithostatic stress under the deformed lithosphere and the averaged lithostatic stress determined in the lowland region down to the same depth, i.e., to the base of the deforming lithosphere (Artyushkov 1973; Turcotte 1983; Molnar & Lyon-Caen 1988). The depth-averaged strength at the imposed nominal strain rate is  $|\sigma_{zz} - \sigma_{xx}|$ , the effective differential stress-driving convergence. Hence, the Argand Ratio is simply:

$$AR = \frac{\sigma_{zz} - \sigma_{yy}}{|\sigma_{zz} - \sigma_{xx}|} \quad (16)$$

and constant values of  $AR$  can therefore be mapped as straight lines onto the  $(\sigma_{zz} - \sigma_{yy}) - (\sigma_{zz} - \sigma_{xx})$  plane, as shown in Figure 4. In the definition of the Argand Ratio, the absolute value of  $(\sigma_{zz} - \sigma_{xx})$  is used so that its sign is consistent with prior use of the Argand Number ( $Ar$ ), in which the positive Argand Number drives extension or resists convergence (England & McKenzie 1982; Houseman & England 1986). Figure 5 depicts the evolution of the Argand Ratio through time for our six model lithospheres.

The convergence history of all Archaean models and that of the Phanerozoic model with an anomalously warm geotherm (Phan80) unfolds in two stages (Fig. 3). In the first stage, convergence is accommodated by crustal and lithospheric thickening, with a monotonically decreasing rate of thickening. The duration of this first stage is proportional to the thickness of the initial lithosphere (Fig. 3). In the second



**Fig. 3.** Evolution of the position of the main density interfaces during convergence. In all Archaean models, the continental lithosphere reaches a plateau stage during which the depths of the density interfaces do not change much. The timescale at which this stage is reached is proportional to the initial thickness of the lithosphere. A similar evolution is displayed by Phan80, which in many respects is like the Archaean models. In contrast, the depth of the density interfaces for Phan120 and Phan160 increases at an increasing rate. In these models, the thickening rate increases despite convergence being driven by a decreasing horizontal stress.

stage, convergence continues without significant thickening and even with a slight decrease in the thickness of the SCLM. This near steady-state evolution is maintained for the duration of the convergence. Since convergence is ongoing, shortening in the  $x$ -direction is balanced by extension in the direction perpendicular to convergence. Surface deformation at this stage

would be primarily in the strike-slip mode. It is interesting to note that during convergence the ratio thickness of the crust to that of the SCLM increases only very slightly (Arch80: 0.5–0.56; Arch120: 0.33–0.363; and Arch160: 0.25–0.269) due to the thermal thinning of the SCLM. Therefore, the two-stage evolution described above cannot be the result of a change in the

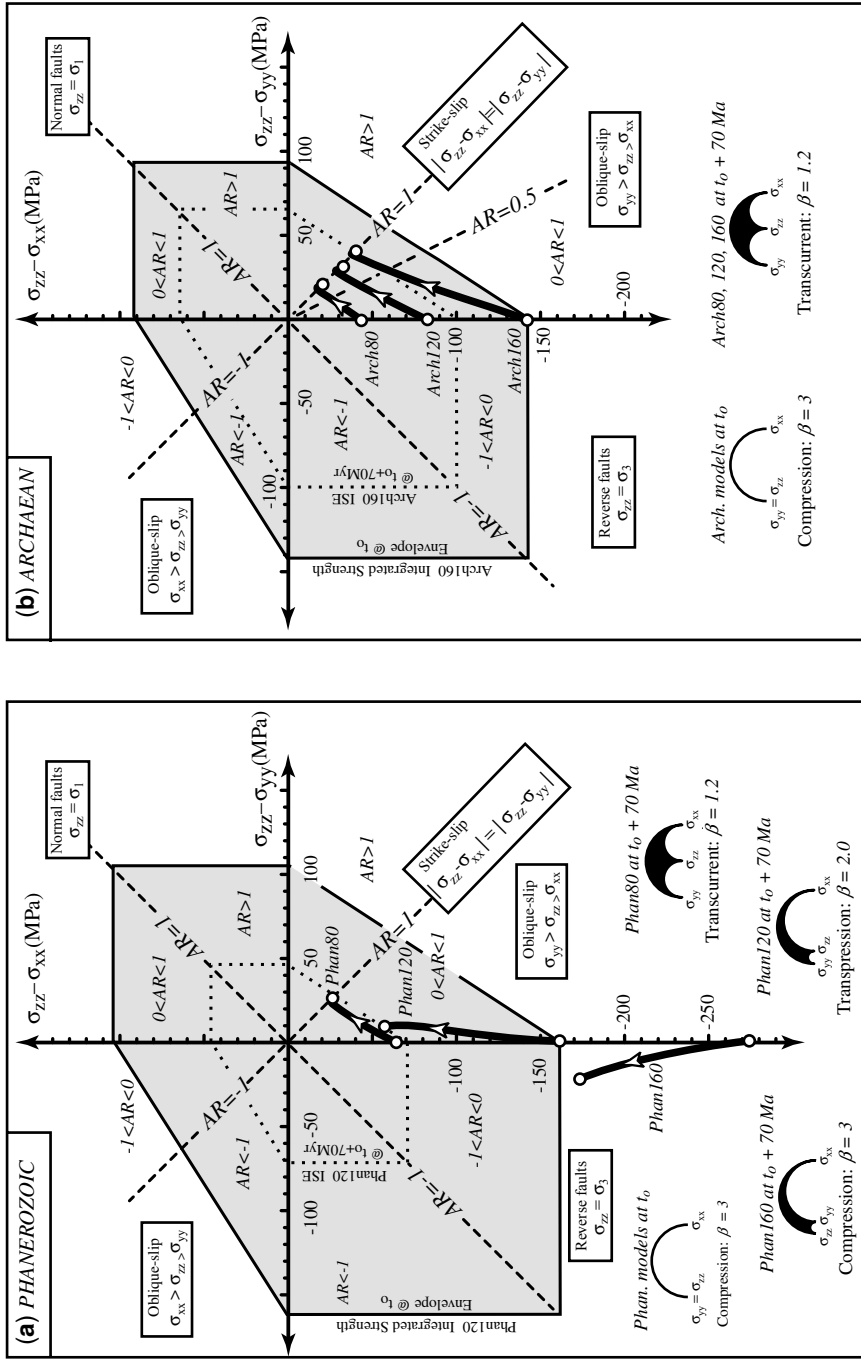


**Fig. 4.** Evolution of the state of stress during convergence is shown on a graph of  $\sigma_{zz} - \sigma_{yy}$  against  $\sigma_{zz} - \sigma_{xx}$  (a) The Phanerozoic model Phan160 follows a stress path within the domain of convergence in both horizontal directions (least principal stress vertical). For the models Phan120 and Phan80 the state of stress is transpressional. (b) The state of stress of all Archaean models becomes transpressional, reaching the transcurrent domain, where  $|\sigma_{zz} - \sigma_{yy}| = |\sigma_{zz} - \sigma_{xx}|$ . Contours parallel to the boundary of the shaded area define the stress differences required to drive deformation at a specified strain-rate. The Argand Ratio (AR) can be mapped into the  $\sigma_{zz} - \sigma_{yy} / \sigma_{zz} - \sigma_{xx}$  plane. The stress state of all Archaean models evolves to an increasingly positive Argand Ratio, eventually reaching 1. At that stage, gravitational stress is equal to the stress that drives convergence.

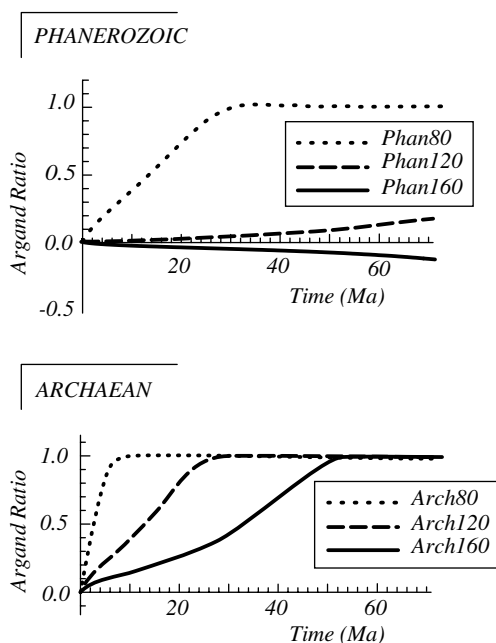


**Fig. 5.** Evolution of the Argand Ratio during convergence. *AR* for all Archaean models evolves toward 1. At that stage, a steady-state evolution is reached where convergence in one horizontal direction is balanced by extension in the orthogonal horizontal direction. Phanerozoic models show variable evolution of *AR*. For Phan60, the gravitational force enhances the tectonically driven convergence, whereas the gravitational force for Phan80 opposes it.

relative thickness of the crustal and the SCLM layers.

Convergence histories for the Phanerozoic models show large variations, that of model Phan80 being similar to that of Archaean models. Convergence histories for Phan120 and Phan160 models follow a different pattern. As shown in Figure 3, the thickening rate increases monotonically, as demonstrated by the progressive deepening of the Moho and that of the isotherm 1330°C. In these cases, the *y*-direction spreading is unable to keep pace with the imposed *x*-direction convergence (Phan120 in Fig. 4) and the increasing gravitational potential energy deficit caused by the thickened lithospheric root actually causes *y*-direction convergence as well (Phan160 in Fig. 4). Eventually this evolutionary path may lead to the initiation of a mechanical instability as the thickening rate increases exponentially, as suggested by Fleitout and Froidevaux (1982). However, as for the Archaean models, the ratio between the

thickness of the crust and that of the SCLM increases very slightly (Phan80: 0.5–0.57; Phan120: 0.33–0.368; and Phan160: 0.25–0.267). The pull of the SCLM is therefore modest.

This contrasting evolution between Archaean and Phanerozoic models is the result of contrasting tectonic regimes that develop in response to an evolving stress balance. Figure 4 illustrates the differences. From its starting point on the biaxial compression axis ( $\sigma_{xx} > \sigma_{zz} = \sigma_{yy}$ , Fig. 4a), the state of stress for the model Phan160 moves into the domain in which both horizontal axes are convergent along a path where  $\sigma_{xx} > \sigma_{yy} > \sigma_{zz}$ . Along that path, the parameter  $\beta = 3$  and the tectonic regime is in contraction. For such a state of stress, it is inferred that reverse faults and thickening would accommodate the convergence. The state of stress for Phan80 and Phan120 follows a path into the transpression domain where  $\sigma_{xx} > \sigma_{zz} > \sigma_{yy}$ . However, after 70 Ma of convergence the parameter  $\beta$  for Phan120 is only 2 (oblique-slip faults), whereas it stabilizes at 1.2 (transcurrent tectonic regime with strike-slip faults) for Phan80. The crustal thickening factors  $f_c$  increase at an increasing rate for Phan120 and Phan160 but stabilize at *ca.* 1.4 for Phan80. All Archaean lithospheres follow a state of stress history similar to that of model Phan80 (Fig. 4b). Their state of stress moves along a transpression path where  $\sigma_{xx} > \sigma_{zz} > \sigma_{yy}$ , and then stabilizes in the transcurrent tectonic regime where  $(\sigma_{xx} - \sigma_{zz}) = (\sigma_{zz} - \sigma_{yy})$ . When the steady-state transcurrent tectonic regime is reached, we infer that strike-slip faults in the upper crust and lateral viscous flow in the lower crust accommodate convergence. This overall lateral flow explains the limited thickening of Archaean lithospheres ( $1.4 \leq f_c \leq 2$ ) and anomalously warm Phanerozoic lithospheres ( $f_c \leq 1.4$ ).

This contrasting evolution is also illustrated by the evolution of the Argand Ratio (Fig. 5). For the Archaean models, and for Phan80, stage 1 of the convergence history leads to a positive Argand Ratio that increases approximately linearly with time (Fig. 5). As the differential stresses have opposite signs they promote opposing flows. Hence, when the Argand Ratio reaches unity (second stage), the tendency of the thickened crust to spread under gravity produces a lateral flow whose rate balances that of convergence, preventing further thickening. In contrast, convergence of the Phanerozoic model Phan160 produces a negative Argand Ratio that decreases at an increasing rate. The gravitational force in this example enhances the tectonic differential stress promoting convergence and thickening. In Phan160, the colder and denser SCLM keel

pulls on the deforming lithosphere, enhancing the compressive horizontal stress and promoting thickening. The role of the SCLM in this kind of instability has been proposed in a number of studies (e.g., Fleitout & Froideveaux 1982; Sun & Murrell 1994; Houseman & Molnar 1997, 2001; Conrad 2000), and England & Houseman (1989) noted that the question of whether increased thickening of the lithosphere leads to an increasingly negative or increasingly positive Argand Ratio depends sensitively on assumed density and thermal parameters. Based on the compositional buoyancy of surviving Archaean SCLM, such instabilities would be less likely in Archaean times, and orogeny would more likely lead to convergence in one direction being balanced by extension in the orthogonal direction.

### Discussion

Because of the secular cooling of the continental geotherm and the secular change in the composition of the SCLM (Griffin *et al.* 1998), continental thickening in modern and Phanerozoic lithospheres develops with typically lower Argand Ratios compared to those of Archaean times. For moderate to cold thermal regimes, prevalent in Phanerozoic and modern continental lithospheres,  $AR$  is  $\ll 1$ , promoting strain localization necessary for the formation of linear orogens (i.e., mountain belts). During thickening, one could expect that high temperature transient continental geotherms (a response to crustal thickening) would lead to an increasing Argand Ratio. This is because warmer conditions increase the buoyancy of the lithosphere (i.e., increase the  $AR$  numerator) while decreasing its integrated strength (i.e., decreasing  $AR$  denominator). However, as shown by our experiments Phan120 and Phan160 (Fig. 3) this effect competes with the cooling of the geotherm induced by the downward heat advection driven by thickening. In Phanerozoic and modern continental lithospheres, Argand Ratios  $\geq 1$ , necessary for the development of extensional collapse, require a change in the external factors that affect the orogen. Such changes may be produced either by a decrease of the driving tectonic stresses (reduction of the  $AR$  denominator), or by a sudden increase in gravitational potential energy induced by the convective thinning of the thermal boundary layer (England & Houseman 1988, 1989) and the establishment of higher transient continental geotherm (increase of  $AR$  numerator). The Basin and Range Province (Jones *et al.* 1996;

Flesch *et al.* 2000) and Tibet (England & Molnar 1997) confirm that, in present-day continental lithospheres, gravitational forces indeed play a significant role in the tectonic evolution of anomalously warm and/or buoyant lithospheres. The convergence experiment Phan80 (Fig. 3) illustrates the impact of gravitational force on an initially warm thin continental lithosphere.

Triaxial numerical experiments clearly point toward a more significant role for gravitational forces in lithospheric deformation during the Archaean. The gravitational forces determine the sustainable amount of thickening, the tectonic regime, and the spatial distribution of strain. The reduced ability of continental lithospheres in the Archaean to sustain significant contrast in gravitational potential energy has profound implications on the mode of deformation during both extensional and contractional deformation. In particular, our triaxial tests suggest that convergence involving warm and buoyant lithospheres would result in (1) less topographic relief, (2) more homogeneous lithospheric deformation distributed over broad regions (i.e., less prominent linear belts), and (3) an overall transcurrent tectonic regime where strike-slip faults and crustal-scale gravitational flow are the likely outcomes of sustained convergence. Experiments performed under driving tectonic forces that produce initial strain rates of  $5 \times 10^{-16} \text{ s}^{-1}$  and  $5 \times 10^{-14} \text{ s}^{-1}$  (Fig. 3) show that these conclusions are not affected by considering different level of tectonic forcing in the Archaean.

Archaean geological records provide plenty of observations consistent with the predictions made above. A low surface elevation and the absence of large gradients of crustal thickness in Archaean cratons are suggested by the rather low and homogeneous erosion level ( $5 \pm 2 \text{ km}$ ) across most Archaean cratons (Galer & Metzger 1998). In particular, the co-existence of very low-grade greenstones in close proximity with granitic domes suggests that in most cases only a few kilometres of supracrustal rocks have been removed by erosion. Hence, erosion does not reveal any deep orogenic zones, but instead reveals low to medium grade meta-sedimentary and meta-volcanic rocks. The evidence of Archaean high-grade terranes such as the Pikwitonei and Kapuskasing domains in the Superior Province, the granulite facies migmatite from the Limpopo belt, and the granulite gneisses of the Karelian craton in central Finland have sometimes been advanced as an argument that regional crustal thicknesses on the order of 60–80 km

were created by Archaean orogenies. These rocks, however, record pressures lower than 1100 MPa (*c.* <40 km) and have been exposed to the surface following Proterozoic exhumation (Percival & Peterman 1994; Kamber *et al.* 1995, 1996; Korsman *et al.* 1999), not during Archaean orogenesis involving crustal-scale thrusts. Crustal-scale gravitational flow is also suggested by the maintenance of a sub-aerial to shallow sub-aqueous surface topography during the accumulation of volcano-sedimentary sequences (greenstones), some up to 20 km thick, above mainly felsic basement (Arndt 1997; De Witt & Ashwal 1997). Despite their thickness, greenstone covers failed to thicken the continental crust sufficiently to raise its surface elevation above sea level. The gravitational flow of the lower continental crust during the loading of crust could explain why the accumulation of thick volcano-sedimentary sequences did not translate into significant crustal thickening or significant gradients in crustal thickness.

The triaxial tests presented here suggest that Archaean continental lithospheres reach the plateau stage, and an Argand Ratio close to one, for a smaller amount of thickening. How much smaller depends on the thickness of the SCLM relative to that of the crust. For Arch120 the plateau stage is reached for a crustal thickening factor of 1.5. Therefore, continental convergence in the Archaean, if sustained, should ultimately have led to orogenies being dominated by strike-slip faults and lateral flow. Crustal-scale thrusts of Archaean age appear absent, and have yet to be documented in Archaean cratons. In contrast, craton-scale strike-slip faults of Archaean age are ubiquitous in many Late Archaean cratons such as the Superior Province, the Yilgarn craton, the Dharwar craton, or the Karilian craton. In the Yilgarn craton for instance, they are typically 50–250 km long and 2–10 km in width (Whitaker 2001). These strike-slip faults develop in close temporal relationship with elliptical granitic intrusions whose long axes roughly parallel the trend of strike-slip faults (e.g., Gee 1979). This structural relationship has previously been used to argue for horizontal shortening accommodated by strike-slip faults and horizontal extension (e.g., Treloar & Blenkinsop 1995; Hamilton 1998; Davis & Maiden 2003). The relatively high spatial frequency of these faults (one to three *c.* 300 km long strike-slip fault every 50 km across strike in the Yilgarn craton) contrasts strongly with the few major faults that accommodate lateral escape tectonics in Phanerozoic and modern convergent orogens such as the Himalayas, the European Alps or the

European Variscan belt. The relatively homogeneous deformation fields of the Archaean are more likely to have extended over greater areas than in Phanerozoic orogenies. With the possible exception of the Superior Province, many Archaean cratons record regional finite strain fields with similar characteristics over a length scale of hundred of kilometres (Choukroune *et al.* 1997; Hamilton 1998), with little or no metamorphic gradient, and little or no tectono-magmatic age gradient. This strongly contrasts with modern orogens where tectono-metamorphic and magmatic events are known to migrate from hinterland to foreland over many tens of millions years.

### Conclusion

The steady-state thermal structure of continental lithospheres in the Archaean may have been similar to that of modern and thermally mature orogenic zones. Studies of present-day crustal flow in Tibet and in the Basin and Range Province argue that gravitational forces play a significant role. Both regions have a high Argand Ratio relative to a large anomaly in gravitational potential energy (particularly in Tibet) and a weak lithosphere (particularly in the Basin and Range Province). In ancient continental lithospheres, warmer steady-state thermal conditions combined with a more buoyant SCLM would have ensured the dominant role of the gravitational force in Archaean continental dynamics. Our numerical experiments show that, because of their contrasted thermo-mechanical properties, Archaean-like (warm and buoyant) and Phanerozoic-like (colder and heavier) continental lithospheres evolve along contrasted strain/stress paths when submitted to the same triaxial deformation conditions. In Archaean times, gravitational forces acted as a stabilizing agent by impeding thickening and promoting diffuse deformation over large areas through gravitational flow perpendicular to the direction of convergence. For moderate to cold thermal regimes, prevalent in Phanerozoic and modern times, the continental lithosphere may be too strong to be impacted by gravitational forces. Only when transient high-temperature geotherms are established do gravitational forces intervene in lithospheric deformation. Secular cooling of the continents has increased their strength while the secular increase in density of the sub-continental lithospheric mantle has reduced their buoyancy, both effects diminishing AR and therefore the relative importance of gravitational forces in continental dynamics.

Many thanks to Y. Poujdom Djomani, B. Griffin and S. O'Reilly for enlightening discussions on the evolution through time of the density of the SCLM. Thanks to S. Buitter, S. Costa, R. Pysklywec and M. Sandiford for their constructive comments of the first draft of this manuscript. Special thanks are due to K. Stüwe whose thorough review considerably improved its final version. This work was supported by ARC Large Grant N<sup>o</sup>: A10017138.

## References

- ARNDT, N. 1997. Why was flood volcanism on submerged continental platforms so common in the Precambrian? *Precambrian Research*, **97**, 155–164.
- ARTYUSHKOV, E. V. 1973. Stresses in the lithosphere caused by crustal thickness inhomogeneities. *Journal of Geophysical Research*, **78**, 7675–7708.
- BAILEY, R. C. 1999. Gravity-driven continental overflow and Archaean tectonics. *Nature*, **398**, 413–415.
- BINNS, R. A., GUNTORPE, R. J. & GROVES, D. I. 1976. Metamorphic patterns and development of greenstone belts in the eastern Yilgarn Block, Western Australia. In: WINDLEY, B. F. (ed.) *The Early History of the Earth*. Wiley, New York, N.Y., 303–316.
- BOUHALLIER, H., CHOUKROUNE, P. & BALLEVRE, M. 1993. Diapirism, bulk homogenous shortening and transcurrent shearing in the Archaean Dharwar craton: the Holenarsipur area. *Precambrian Research*, **63**, 43–58.
- BRACE, W. F. & KOHLSTEDT, D. L. 1980. Limits on lithospheric stress imposed by laboratory experiments. *Journal of Geophysical Research*, **85**, 6248–6252.
- BUCK, W. R. & SOKOUTIS, D. 1984. Analogue model of gravitational collapse and surface extension during continental convergence. *Nature*, **369**, 737–740.
- CHARDON, D., CHOUKROUNE, P. & JAYANANDA, M. 1998. Sinking of the Dharwar Basin (South India); implications for Archaean tectonics. *Precambrian Research*, **91**, 15–39.
- CHOUKROUNE, P., BOUHALLIER, H. & ARNDT, N. T. 1995. Soft lithosphere during periods of Archaean crustal growth or crustal reworking. In: COWARD, M. P. & RIES, A. C. (eds) *Early Precambrian Processes*. Geological Society, London, Special Publications, **95**, 67–86.
- CHOUKROUNE, P., LUDDEN, J. N., CHARDON, D., CALVERT, A. J. & BOUHALLIER, H. 1997. Archaean crustal growth and tectonic processes: a comparison of the Superior Province, Canada and the Dharwar Craton, India. In: BURG, J. P. & FORD, M. *Orogeny Through Time*. Geological Society, London, Special Publications, **121**, 63–98.
- COLLINS, W. J. 1989. Polydiapirism of the Archaean Mount Edgar Batholith, Pilbara Block, Western Australia. *Precambrian Research*, **43**, 41–62.
- CONRAD, C. P. 2000. Convective instability of thickening mantle lithosphere. *Geophysics Journal International*, **143**, 52–70.
- DAVIS, B. K. & MAIDEN, E. 2003. Archaean orogen-parallel extension: evidence from the northern Eastern Goldfields Province, Yilgarn Craton. *Precambrian Research*, **127**, 229–248.
- DE WITT, M. & ASHWALL, L. D. 1997. Greenstone Belts. *Oxford Monographs on Geology and Geophysics*, **35**.
- ENGLAND, P. C. & HOUSEMAN, G. A. 1988. The mechanics of the Tibetan plateau. *Philosophical Transactions of the Royal Society of London*, **326**, 301–320.
- ENGLAND, P. C. & HOUSEMAN, G. A. 1989. Extension during continental convergence, with application to the Tibetan Plateau. *Journal of Geophysical Research*, **94**, 17561–17579.
- ENGLAND, P. C. & MCKENZIE, D. P. 1982. A thin viscous sheet model for continental deformation. *Geophysical Journal of the Royal Astronomical Society*, **70**, 295–321.
- ENGLAND, P. C. & MCKENZIE, D. P. 1983. Correction to: A thin viscous sheet model for continental deformation. *Geophysical Journal of the Royal Astronomical Society*, **73**, 523–532.
- ENGLAND, P. C. & MOLNAR, P. 1997. Active deformation of Asia: from kinematics to dynamics. *Science*, **278**, 647–650.
- EVANS, B. & GOETZE, C. 1979. The temperature variation of hardness of olivine and its implication for polycrystalline yield stress. *Journal of Geophysical Research*, **84**, 5505–5524.
- FLEITOUT, L. & FROIDEVAUX, C. 1982. Tectonics and topography for a lithosphere containing density heterogeneities. *Tectonics*, **1**, 21–56.
- FLESCH, L. M., HOLT, W. E., HAINES, A. J. & SHEN-TU, B. 2000. Dynamics of the Pacific-North American plate boundary in the western United States. *Science*, **287**, 834–836.
- GALER, S. & METZGER, K. 1998. Metamorphism, denudation and sea level in the Archaean and cooling of the Earth. *Precambrian Research*, **92**, 389–412.
- GEE, R. D. 1979. Structure and tectonic style of the Western Australia shield. *Precambrian Research*, **58**, 327–369.
- GRIFFIN, W. L., O'REILLY, S. Y., RYAN, C. G., GAUL, O. & IONOV, D. 1998. Secular variation in the composition of the subcontinental lithospheric mantle. In: BRAUN, J. ET AL. (eds) *Structure and Evolution of the Australian Continent*, Geodynamics Series, **26**, American Geophysical Union, 1–25.
- HAMILTON, W. B. 1998. Archean magmatism and deformation were not products of plate tectonics. *Precambrian Research*, **91**, 143–179.
- HOUSEMAN, G. & ENGLAND, P. 1986. Finite strain calculations of continental deformation: 1. Method and general results for convergent zone. *Journal of Geophysical Research*, **91**, 3651–3663.
- HOUSEMAN, G. & MOLNAR, P. 1997. Gravitational (Rayleigh-Taylor) instability of a layer with non-linear viscosity and convective thinning of continental lithosphere. *Geophysics Journal International*, **128**, 125–150.
- HOUSEMAN, G. & MOLNAR, P. 2001. Mechanisms of lithospheric renewal associated with continental orogeny. In: MILLER, J. A., HOLDSWORTH, R. E., BUICK, I. S. & HAND, M. (eds) *Continental Reworking and Reactivation*. Geological Society, London, Special Publications, **184**, 13–37.

- JELSMA, H. A., VAN DER BEEK, P. A. & VINYU, M. L. 1993. Tectonic evolution of the Bindura-Shamva greenstone belt (northern Zimbabwe): progressive deformation around diopiric batholiths. *Journal of Structural Geology*, **15**, 163–176.
- JONES, C. H., UNRUH, J. R. & SONDER, L. J. 1996. The role of gravitational potential energy in active deformation in the southwestern United States. *Nature*, **381**, 37–41.
- KAMBER, B. S., BIINO, G. G., WIJBRANS, J. R., DAVIES, G. R. & VILLA, G. 1996. Archaean granulites of the Limpopo Belt, zone of the Limpopo Belt, Zimbabwe: one slow exhumation or two rapid events? *Tectonics*, **15**, 1414–1430.
- KAMBER, B. S., KRAMERS, J. D., NAPIER, R., CLIFF, R. A. & ROLLINSON, H. R. 1995. The Triangle Shearzone, Zimbabwe, revisited: new data document an important event at 2.0 Ga in the Limpopo Belt. *Precambrian Research*, **70**, 191–213.
- KORSMAN, K., KORJA, T., PAJUNEN, M., VIRRANSALO, P. & GGT/SVEKA WORKING GROUP, 1999. The GGT/SVEKA Transect – structure and evolution of the continental crust in the Palaeoproterozoic Svecofennian Orogen in Finland. *International Geology Review*, **41**, 287–298.
- LENARDIC, A. & MORESI, L. 2000. A new class of equilibrium geotherms in the deep thermal lithosphere of continents. *Earth Planetary Science Letters*, **176**, 331–338.
- MCGREGOR, A. M. 1951. Some milestones in the Precambrian of Southern Rhodesia. *Transactions of the Geological Society of South Africa*, **54**, 27–70.
- MOLNAR, P. & LYON-CAEN, H. 1988. Some simple physical aspects of the support, structure and evolution of mountain belts. In: CLARK JR., S. P., BURCHFIELD, B. C. & SUPPE, J. (eds) *Processes in Continental Lithosphere Deformation*. Geological Society of America, Special Papers, **218**, 179–207.
- MOLNAR, P., HOUSEMAN, G. A. & CONRAD, C. P. 1998. Rayleigh-Taylor instability and convective thinning of mechanically thickened lithosphere: effects of non-linear viscosity decreasing exponentially with depth and of horizontal shortening of the layer. *Geophysical Journal International*, **133**, 568–584.
- MYERS, J. & WATKINS, K. P. 1985. Origin of granite-greenstone patterns, Yilgarn Block, Western Australia. *Geology*, **13**, 778–780.
- PERCIVAL, J. A. & PETERMAN, Z. E. 1994. Rb–Sr biotite data from the Kapuskasing uplift and their bearing on the cooling and exhumation history. *Canadian Journal of Earth Sciences*, **31**, 1172–1181.
- QIU, Y. M., MCNAUGHTON, N. J., GROVES, D. I. & DALSTRA, H. J. 1999. Ages of internal granitoids in the Southern Cross region, Yilgarn Craton, Western Australia, and their crustal evolution and tectonic implications. *Australian Journal of Earth Sciences*, **46**, 971–981.
- RAMSAY, J. G. 1989. Emplacement kinematics of a granite diapir: the Chindamora batholith, Zimbabwe. *Journal of Structural Geology*, **11**, 191–209.
- RANALLI, G. 1995. *Rheology of the Earth*. Chapman & Hall, London.
- REY, P., PHILIPPOT, P. & THÉBAUD, N. 2003. Contribution of mantle plume, crustal thickening, and greenstone blanketing to the 2.75–2.65 Ga global crisis. *Precambrian Research*, **127**, 43–60.
- SCHMALHOLZ, S. M., PODLADCHIKOV, Y. Y. & BURG, J. P. 2002. Control of folding by gravity and matrix thickness: implications for large-scale folding. *Journal of Geophysical Research*, **107**, no B1, ETG-1–1, DOI 10.1029/2001JB000355.
- SCHMALHOLZ, S. M., PODLADCHIKOV, Y. Y. & JAMVIET, B. 2005. Structural softening of the lithosphere. *Terra Nova*, **17**, 66–72.
- SIBSON, R. H. 1974. Frictional constraints on thrust, wrench and normal faults. *Nature*, **249**, 542–544.
- SONDER, L. J., ENGLAND, P. C., WERNICKE, B. P. & CHRISTIANSEN, R. L. 1987. A physical model for Cenozoic extension of the western North America. In: COWARD, M. P., DEWEY, J. F. & HANCOCK, P. L. (eds) *Continental Extensional tectonics*. Geological Society, London, Special Publications, **28**, 187–201.
- SNOWDEN, P. A. & BICKLE, M. J. 1976. The Chindamora Batholith; diapiric intrusion of interference fold? *Journal of the Geological Society, London*, **132**, 131–137.
- SUN, J. & MURRELL, A. F. 1994. On the growth and collapse of wide orogenic belts. *Geophysical Journal International*, **118**, 255–268.
- TAYLOR, S. R. & MCLENNAN, S. M. 1986. The chemical composition of the Archaean crust. In: DAWSON, J. B., CARSWELL, D. A., HALL, J. & WEDEPOHL, K. H. (eds) *The Nature of the Lower Continental Crust*. Geological Society, London, Special Publications, **24**, 173–178.
- TREOLAR, P. J. & BLENKINSOP, T. G. 1995. Archaean deformation patterns in Zimbabwe: true indicators of Tibetan-style crustal extrusion or not? In: COWARD, M. P. & RIES, A. C. (eds) *Early Precambrian Processes*. Geological Society, London, Special Publications, **95**, 87–107.
- TURCOTTE, D. L. 1983. Mechanisms of crustal deformation. *Journal of the Geological Society, London*, **140**, 701–724.
- WARREN, R. G. & ELLIS, D. J. 1996. Mantle-underplating, granite tectonics, and metamorphic P–T–t paths. *Geology*, **24**, 663–666.
- WHITAKER, A. J. 2001. Component and structure of the Yilgarn craton, as interpreted from aeromagnetic data. 4th International Archaean Symposium 2001, Extended Abstracts. In: CASSIDY, K. F. ET AL. (eds) 2001. *AGSO–Geoscience Australia, Record*, **37**, 536–538.

